Biogeochemical processes and arsenic enrichment around rice roots in paddy soil: Results from micro-focused X-ray spectroscopy

J. FROMMER [a], A. VOEGELIN[b], J. DITTMAR [a], M. A. MARCUS[c], R. KRETZSCHMAR [a]

[a]*Soil Chemistry Group, Institute of Biogeochemistry and Pollutant Dynamics, ETH Zurich, CHN, CH-8092 Zurich, Switzerland.*

[b]*Eawag, Swiss Federal Institute of Aquatic Science and Technology, Ueberlandstrasse 133, CH-8600 Duebendorf, Switzerland*

[c]*Advanced Light Source, Lawrence Berkeley National Laboratory, MS 6-2100, Berkeley, CA 94720, USA,*

Correspondence: A. Voegelin. E-mail: andreas.voegelin@eawag.ch .

Supporting Information

(11 pages, 1 table, 4 figures)

S1 XAS and XRF analysis 2

S2 Iron reference compounds 5

S3 X-ray diffraction analysis of the topsoil sample 7

S4 Fe K-edge XANES LCF 8

S5 Additional figures 10

Literature cited 11

S1 XAS and XRF analysis

XAS data evaluation

For the Fe data, we fixed E_0 to 7128 eV, subtracted a linear pre-edge function fitted between 7028 and 7098 eV, and normalized the data to unit edge jump by extrapolating a second-order polynomial fitted between 7178 and 7698 eV to E_0.

For the Mn data we fixed E_0 to 6550 eV, subtracted a linear pre-edge function fitted between 6450 and 6520 eV, and normalized the data to unit edge jump by extrapolating a first-order polynomial fitted between 6600 and 6830 eV to E_0. The normalized XANES spectrum of the bulk soil was analyzed by LCF using reference spectra of dissolved Mn^{2+} (50 mM $MnCl_2$), ripidolite (natural specimen, source clay CCa-2, containing mainly Mn(III)), and Na-birnessite (synthesized as described elsewhere (Jacquat *et al.*, 2008), but without addition of Zn) as fit components (energy range of the fit: 6535-6580 eV).

For the As data we fixed E_0 to 11871 eV, subtracted a linear pre-edge function fitted between 11771 and 11856 eV, and normalized the data to unit edge jump by extrapolating a first-order polynomial fitted between 11971 and 12171 eV to E_0. The average As oxidation state in the soil sample was determined by LCF of the normalized XANES using the normalized XANES spectra of As(III) and As(V) adsorbed to ferrihydrite (Voegelin *et al.*, 2007) (energy range: 11851-11901 eV) and by LCF of the EXAFS spectrum using the same references (*k*-range: 3-8 $Å^{-1}$).

Micro-focused X-ray analysis

To reduce beam-induced speciation changes, the soil sections were mounted on a Peltier cooling stage (surface temperature: ~27°C; dry N_2 atmosphere to prevent ice formation) in a 45° angle to the incident beam, and the fluorescence signal was recorded in a 90° angle using a Ge 7-element solid state detector. Distribution maps for As and Fe were collected with an incident photon energy

of 13 keV. Maps for Mn were measured with an incident photon energy of 7 keV to prevent leakage of Fe K_α fluorescence into the Mn channel. Evaluation of the μ-XRF mapping-data was done by software developed at ALS beamline 10.3.2. For all element maps shown, the black-level was set to 0 counts and the white-level to the 98th percentile (i.e., 98% of the pixels have an intensity smaller or equal to the white-level). Furthermore, we calculated distribution maps for the XRF-derived molar As/Fe ratios. Before calculating the ratio of the respective XRF channels, we subtracted a background level (resulting from scattering and sample fluorescence other than As K_α-fluorescence) from the As channel counts. This background level was determined by averaging the count-rate in the As channel at several spots in the soil matrix (i.e., away from roots) for which the full XRF spectrum indicated the absence of As K_α fluorescence. To convert this intensity ratio into a molar ratio, we determined a conversion factor as described in the next paragraph.

The sections are polished to a thickness of about 30 μm. Considering the 45° angle of incidence of incoming and outgoing X-rays this sample thickness corresponds to a maximum pathlength of 42 μm (one-way) in the sample. Assuming an average bulk soil density of 1 g cm^{-3} (Dittmar *et al.*, 2007) and using the average elemental composition of the topsoil matrix as determined by bulk XRF analysis, we calculate an absorption length of 110 μm and 750 μm for photon-energies of 5.9 keV (Mn K_α-fluorescence) and 13 keV (excitation energy used for XRF imaging), respectively (cross-sections from Elam database). The path-lengths in the sample are thus well below the absorption length of the relevant excitation and fluorescence energies and we conclude that the thin-layer approximation can be applied. To calculate the (matrix independent) factor for the conversion of Fe/As XRF-intensity ratios into Fe/As mass ratios, we determined the sensitivities (I_0 normalized photon count rate per mass density) of these two elements on foil standards (MICROMATTER™, Vancouver, Canada), with a thin film of Fe (43.9 ± 2.2 μg Fe cm^{-2}) and GaAs (47.8 ± 2.4 μg GaAs cm^{-2}), respectively, deposited onto a Mylar backing. The mass fraction of As in the latter standard was calculated from the fluorescence intensities by using the

tabulated absorption cross-section and the fluorescence yields (Krause, 1979; Elam *et al.*, 2002). The same sample-detector geometry and the same sample-detector distance than for the analysis of the sample sections were used. The calculated sensitivity ratio (sensitivity(As)/sensitivity(Fe)) was 2.57. Thus, experimental As/Fe intensity-ratios can be converted into As/Fe mass-ratios and mole-ratios by a multiplication with a factor of 0.39 and 0.29, respectively.

At selected points of interest (POI), μ-XANES (Fe, Mn, and As) and μ-EXAFS (Fe) spectra were recorded. In general, multiple scans were collected from the same spot. Sporadically, consecutive scans revealed beam-induced reduction of Fe, Mn, and As. In this case, only the first scan was used for further analysis. For As K-edge XAFS, an Al-foil was occasionally placed in front of the detector to mitigate background fluorescence. The Si(111) DCM was calibrated with Fe- and Mn-foil spectra which were aligned to the respective reference spectra of the bulk beamlines. In the case of the As K-edge XAFS spectra, the calibration was done by setting the maximum in the absorption spectrum (whiteline) of As(V) adsorbed to ferrihydrite to 11873.7 eV.

S2 Iron reference compounds

The full set of Fe reference compounds used is listed in Table S1; a subset including only 5 reference compounds was needed to reproduce the experimental spectra. The Fe speciation in the reference compounds of this subset are discussed below:

The two selected Fe(II) containing phyllosilicates, biotite and the source clay reference chlorite CCa-2, are both trioctahedral minerals. The biotite sample contained about 3 wt% Mg and 16 wt% Fe, 87% of which occurs in the form of Fe(II) (Table S1). The next nearest metals around Fe in the octahedral sheet are predominantly Fe atoms as indicated by the intense second shell in the Fourier transformed spectrum (Figure 1c). A quantitative analysis of the Fe K pre-edge XANES spectrum of CCa-2 indicated that 91% of the Fe is present as Fe(II), which agrees well with the Fe(II) fraction (90%) determined in a Mössbauer spectroscopic study of the related reference clay CCa-1 (Drodt *et al.*, 1997). The weaker second shell peak in the Fourier transform and the higher Mg content (6.5 wt%) indicate that the number of next nearest iron neighbors is smaller for CCa-2 than for the biotite reference.

The two Fe(III) containing phyllosilicates, the source clay reference illite IMt-1 and smectite SWy-2, are both dioctahedral minerals. They differ in the total Fe content (IMt-1: 5 wt% Fe, SWy-2: 3 wt% Fe) and in the number of next-nearest-iron neighbors: while on the average 1 out of 4 octahedral metals/metalloids in IMt-1 is an Fe (O'Day *et al.*, 2004), no Fe nearest neighbor is present in SWy-2 (Vantelon *et al.*, 2003). Furthermore the FeO_6 octahedron in SWy-2 is less distorted than in IMt-1. IMt-1 has been shown to be a good proxy for Fe(III) bound in micaceous minerals (O'Day *et al.*, 2004).

Two-line ferrihydrite is a poorly crystalline Fe oxyhydroxide which is commonly formed in pedogenic environments (Cornell & Schwertmann, 2003; Rancourt *et al.*, 2005). Ferrihydrite and its varieties are also formed under biological control (e.g. ferritin, b-HFO). 2-line ferrihydrite serves as a proxy for the class of Fe (oxyhydr-)oxides (O'Day *et al.*, 2004).

Table S1. Fe reference compounds used for the linear combination fitting

name	group	Fe/Me_o[§] (%)	Fe(II) (%)	type	beamline	source
biotite	Fe(II)-ps	71	87[†]	natural	HASYLAB A1	isolate from granite obtained from M. Kiczka
chlorite (CCa-2)	Fe(II)-ps	52	91[†]	natural	HASYLAB C	Source Clay Repository
smectite (SWy-2)	Fe(III)-ps	15	7[‡]	natural	HASYLAB C	Source Clay Repository
illite (IMt-1)	Fe(III)-ps	21	12[†]	natural	HASYLAB C	Source Clay Repository
2-line ferrihydrite	ox	-	0[*]	synthetic	HASYLAB A1	
goethite	ox	-	0[*]	synthetic	ANKA XAS	obtained from O. Jacquat
maghemite	ox	-	0[*]	synthetic	HASYLAB A1	obtained from J. Wiederhold
magnetite	ox	-	33[*]	natural	HASYLAB A1	isolate form granite obtained from M. Kiczka
siderite	carb	-	100[*]	natural	ANKA XAS	obtained from mineral collection of ETH Zurich
pyrite	sulfide	-	100[*]	natural	ANKA XAS	obtained from mineral collection of ETH Zurich
FeS	sulfide	-	100[*]	chemical	ANKA XAS	Fluka 44995
$Fe(II)SO_4(aq)$	Fe(II) (aq)	-	100[*]	chemical	ANKA XAS	

Abbreviations: ps: phyllosilicate; ox: oxide / oxyhydroxide; carb: carbonate; rep: repository.
[§]amount of Fe divided by the total amount of cations in the octahedral sheet; this fraction was approximated by the Fe/(Fe+Mg) ratio for the Fe(II)-ps samples and the $Fe/(Fe+Al_{oct})$ ratio for the Fe(III)-ps samples. The data are derived from own XRF measurements (Fe(II)-ps) and from the stoichiometric data given by Vantelon et al., 2003 (Fe(III)-ps), respectively. [†]Estimated from pre-edge barycenter position according to a method described by Wilke et al., 2001. [‡] No high energy resolution data were available for an experimental determination. Thus the Fe(II) content of SWy-2 was estimated by using the stoichiometric data given in Vantelon et al., 2003. [*]deduced from the stoichiometry.

S3 X-ray diffraction analysis of the topsoil sample

XRD patterns were recorded on a Bruker D4 diffractometer (Cu anode, energy dispersive solid state detector; continuous scans from 4° to 70° 2θ with variable slits). The diffraction pattern was background subtracted and sample height displacement was corrected by aligning the Quartz diffraction pattern in the sample to the one of a standard sample (powder diffraction pattern 00-046-1045).

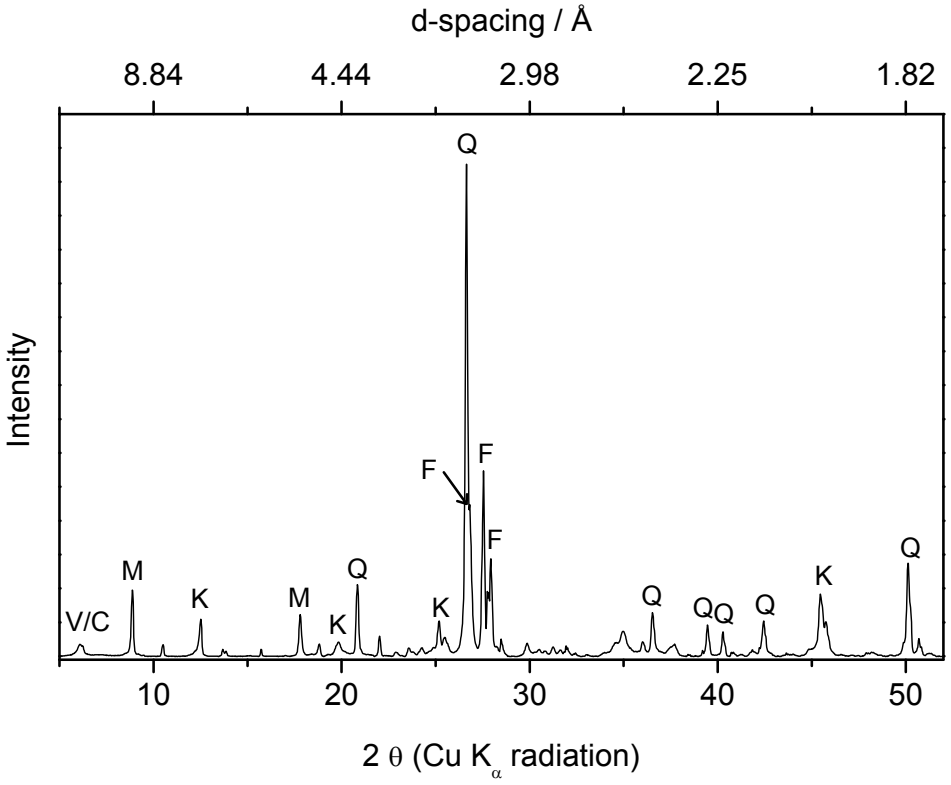

Figure S1. Powder X-ray diffraction pattern of the bulk topsoil sample; M: mica; K: kaolinite; Q: quartz; F: feldspar (Albite, Orthoclase); C: chlorite; V: vermiculite.

S4 Fe K-edge XANES LCF

Figure S2 contains the smoothed first derivative spectra of the samples and references shown in Figure 1. The linear combination fits to the normalized XANES spectra were in general similar to the fit to the first derivative XANES spectra, in that the fitted fractions agreed within about 10% (absolute). Only for the bulk and the matrix spectrum the results of the two approaches differed distinctly. We will briefly discuss the case of the bulk spectrum. The biotite, IMt-1, SWy-2, and 2L-Fh fractions resulting from the fit to the normalized XANES spectrum of the bulk soil were 24%, 40%, 36%, and 0%, respectively. Thus, particularly the SWy-2 and the 2L-Fh fraction differed distinctly between the fits to the derivative and the normal XANES spectrum (normal: SWy-2: 36%, 2L-Fh: 0%; derivative: SWy-2: 2%, 2L-Fh: 29%). As the references did not provide an exact reproduction of the sample spectrum, these differences reflect the different sensitivities of the two approaches; while the fit to the normal spectrum provides a better absolute match particularly in the region of the post-edge peak around 7145 eV, the fit to the derivative spectra better reproduced the overall structure in the XANES spectrum. For our purposes we preferred the latter fit, as the reproduction of the spectral shape ensures that the full spectrum of bonding environments is reflected in the fit, while the intensity can also be influenced by experimental factors of subtle characteristics of the Fe species in the sample which are not reproduced in the reference spectra.

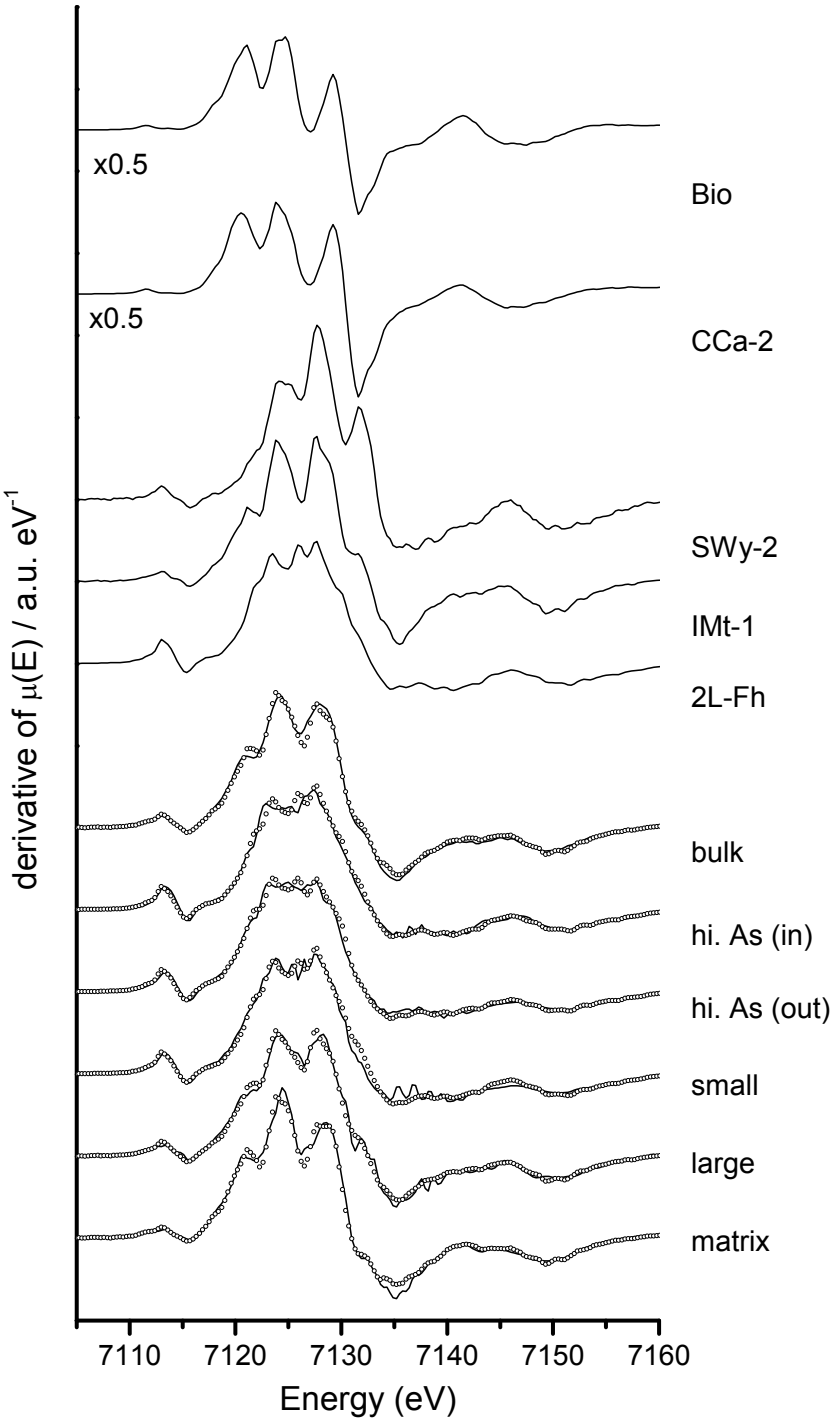

Figure S2. smoothed first derivative of the normalized sample and reference XANES spectra shown in Figure 1. The derivative spectra of Bio and CCa-2 were scaled by 0.5. In addition the LCF fits to the sample spectra are shown (open dots).

S5 Additional figures

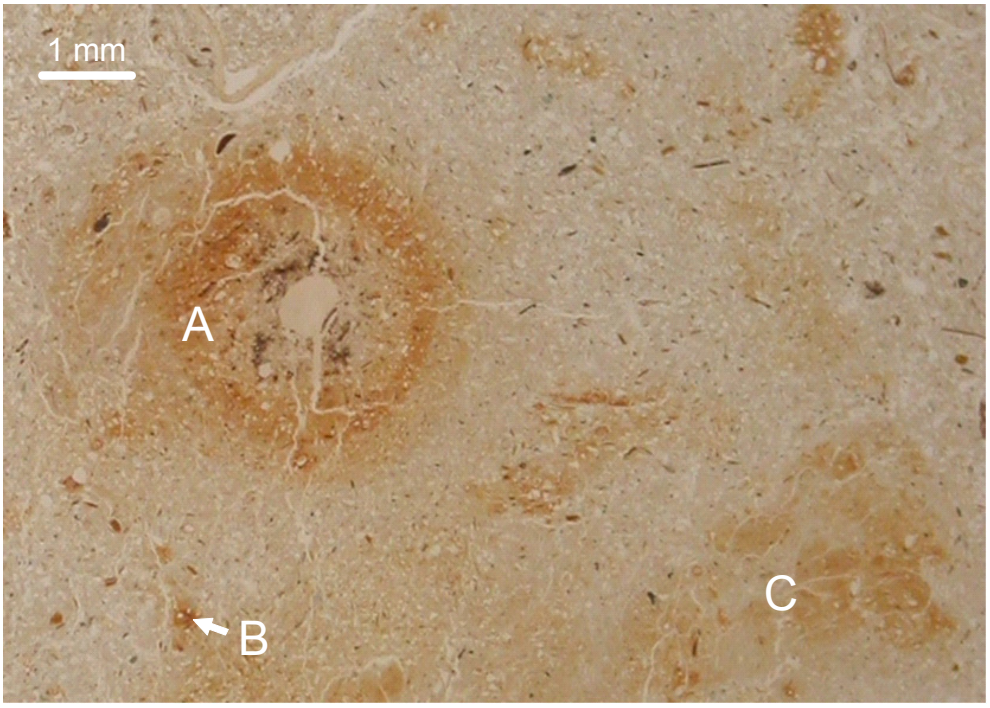

Figure S3. Light microscope image of a soil thin section showing a large (A) and a small (B) concentric element enrichment pattern and a diffuse accumulation of Fe(III) precipitates (C). An approximate scale bar is shown.

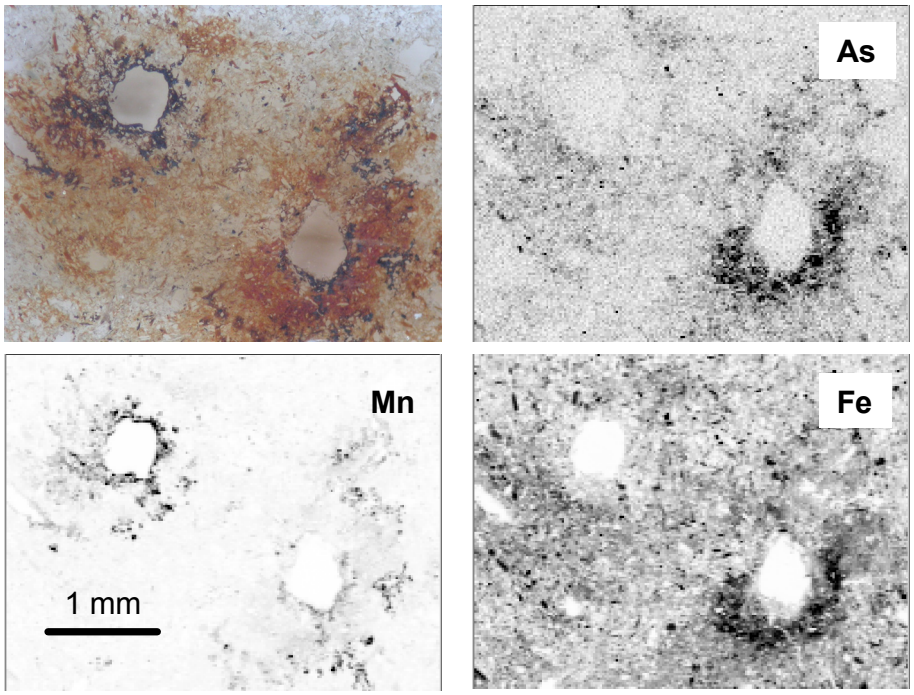

Figure S4. Light microscope image (top left) of two larger (root) channels, along with the distribution of As, Fe, and Mn (μ-XRF). The sample was collected in a depth between 14 and 16 cm in May 2006.

Literature cited

Cornell, R.M. & Schwertmann, U. 2003. *The Iron Oxides*. Wiley-VCH.

Dittmar, J., Voegelin, A., Roberts, L.C., Hug, S.J., Saha, G.C., Ali, M.A., Badruzzaman A.B.M. & Kretzschmar R. 2007. Spatial distribution and temporal variability of arsenic in irrigated rice fields in Bangladesh. 2. Paddy soil. *Environmental Science & Technology*, **41,** 5967-5972.

Drodt, M., Trautwein, A.X., König, I., Suess, E. & Bender Koch, C. 1997. Mössbauer spectroscopic studies on the iron forms of deep-sea sediments. *Physics and Chemistry of Minerals*, **24,** 281-293.

Elam, W.T., Ravel, B.D. & Sieber, J.R. 2002. A new atomic database for X-ray spectroscopic calculations. *Radiation Physics and Chemistry*, **63,** 121-128.

Jacquat, O., Voegelin, A., Villard, A., Marcus, M.A. & Kretzschmar, R. 2008. Formation of Zn-rich phyllosilicate, Zn-layered double hydroxide and hydrozincite in contaminated calcareous soils. *Geochimica et Cosmochimica Acta*, **72,** 5037-5054.

Krause, M.O. 1979. Atomic radiative and radiationless yields for K-shells and L-shells. *Journal of Physical and Chemical Reference Data*, **8,** 307-327.

O'Day, P.A., Rivera, N., Root, R. & Carroll, S.A. 2004. X-ray absorption spectroscopic study of Fe reference compounds for the analysis of natural sediments. *American Mineralogist*, **89,** 572-585.

Rancourt, D.G., Thibault, P.J., Mavrocordatos, D. & Lamarche, G. 2005. Hydrous ferric oxide precipitation in the presence of nonmetabolizing bacteria: Constraints on the mechanism of a biotic effect. *Geochimica et Cosmochimica Acta*, **69,** 553-577.

Vantelon, D., Montarges-Pelletier, E., Michot, L.J., Briois, V., Pelletier, M. & Thomas, F. 2003. Iron distribution in the octahedral sheet of dioctahedral smectites. An FeK-edge X-ray absorption spectroscopy study. *Physics and Chemistry of Minerals*, **30,** 44-53.

Voegelin, A., Weber, F.-A. & Kretzschmar, R. 2007. Distribution and speciation of arsenic around roots in a contaminated riparian floodplain soil: Micro-XRF element mapping and EXAFS spectroscopy. *Geochimica et Cosmochimica Acta*, **71,** 5804-5820.